

# Around-Corner and Over-Top 28 GHz Measurement in Manhattan: Path Loss and AoA for MU-MIMO

Abhishek Adhikari<sup>1</sup>, Shivan Mukherjee<sup>1</sup>, Aahan Mehta<sup>2</sup>, Manav Kohli<sup>1</sup>, Rodolfo Feick<sup>3</sup>, Reinaldo Valenzuela<sup>4</sup>, Dmitry Chizhik<sup>4</sup>, Jinfeng Du<sup>4</sup>, Gil Zussman<sup>1</sup>

<sup>1</sup>Columbia University, NY, USA; <sup>2</sup>Duke University, NC, USA;

<sup>3</sup>UTFSM, Valparaíso, Chile; <sup>4</sup>Nokia Bell Labs, NJ, USA

Email: <sup>1</sup>{aa4832, sm5155, mpk2138, gz2136}@columbia.edu, <sup>2</sup>aahan.mehta@duke.edu,

<sup>3</sup>rodolfo.feick@usm.cl, <sup>4</sup>{dmitry.chizhik, jinfeng.du, reinaldo.valenzuela}@nokia-bell-labs.com

**Abstract**—This paper presents findings from an extensive 28 GHz mmWave measurement campaign conducted in New York City. The study includes over 20 million power measurements collected from two key scenarios: around-corner (non-line-of-sight due to building blockages) and same-street (nominally line-of-sight without obstructions from street furniture or foliage), covering over 1,300 unique links. For urban macro-cell (UMa) rooftop base stations above local clutter, the dominant angle of arrival (AoA) deviates by only 2 to 3.5 degrees from the direct transmitter/receiver direction. This small deviation allows for effective spatial separation between users, facilitating the future development of Multi-User MIMO algorithms for Beyond-5G networks. In the urban micro-cell (UMi) dataset, with base stations below local clutter, a path gain drop of over 20 dB was observed in around-corner segments just 20 meters into a corner. Our Street-Clutter-NLOS path loss model achieves an RMSE of 6.4 dB, compared to 11.9 dB from NLOS 3GPP models. Using the best path loss model to estimate coverage for 90% of users traveling around corners, downlink rates could drop by over 10 times after 50 meters, highlighting the challenges in maintaining consistent user experience over mmWave networks in urban street canyons.

**Index Terms**—NLOS;Multi-User MIMO; path loss modeling; outdoor coverage

## I. INTRODUCTION

Millimeter-wave (mmWave) communication addresses the critical challenges of spectrum congestion in sub-6 GHz bands. However, mmWave networks face significant challenges, primarily due to high path loss and susceptibility to blockage. Accurate modeling of mmWave signal propagation is essential for the effective design and deployment of these networks. While substantial research has focused on line-of-sight (LOS) scenarios [1]–[14], there is a notable gap in the understanding of non-line-of-sight (NLOS) propagation, particularly in urban environments. Existing models often lack the robustness needed for practical applications, especially when based on limited real-world data [1].

To address this gap, this paper presents findings from an extensive NLOS mmWave measurement campaign we collected in Manhattan, New York City, utilizing the FCC Innovation Zone of the PAWR COSMOS advanced wireless testbed to collect measurements [15]. This study categorizes these measurements into two scenarios: urban macro-cell (UMa) and urban micro-cell (UMi). These scenarios are illustrated in Fig. 1. From 2 UMa and 7 UMi RX locations in Upper

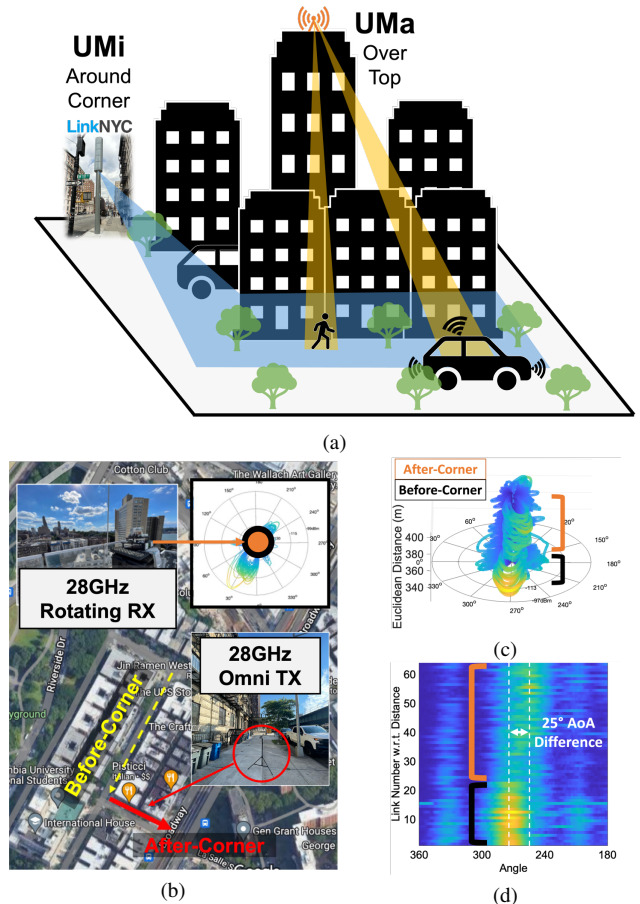


Fig. 1: (a) UMa and UMi scenarios in an urban environment, (b) UMa scenario with rotating 28 GHz receiver as base station and omnidirectional 28 GHz transmitter as user equipment, (c-d) Tracking user equipment with an angle accuracy of 2.0-3.5 degrees before and after turning the corner.

and Lower Manhattan across 3 UMa and 20 UMi routes, we collect a substantial dataset comprising of 14,097,600 NLOS and 6,235,200 LOS individual power measurements. This extensive dataset corresponds to 979 and 433 links.

Using the UMa measurements, we show that a rooftop base station can track user equipment with an angle accuracy of 2.0-3.5 degrees, before and after the user travels to a different street. This can be seen in Fig. 1(c-d) and are elaborated in Section V. These findings offer a level of certainty for considering multi-user MIMO in rooftop deployments. Spatial

TABLE I: Prior NLOS measurement studies in urban/suburban environments in various frequency ranges with various equipment designs.

Ref.	Freq.	TX	RX	Environment	BW	NLOS Links	Elev.
[16]	28 GHz	Omni	Rotating Horn	Urban	Narrowband	75	Balcony
[17]	73.5 GHz	Fixed Horn	Fixed Horn	Urban	1 GHz	16	Street
[18]	28 GHz	Array	Array	Urban	400 MHz	70	Street
[19]	28 GHz	Fixed Horn	Fixed Horn	Urban	250 Mcps	47	Balcony
[20], [21]	28 GHz	Fixed Horn	Rotating Horn	Urban	800 MHz	20	Street
[21]–[23]	38 GHz	Rotating Horn	Rotating Horn	Urban	400 Mcps	18	Street, Rooftop
[24]	142 GHz	Rotating Horn	Rotating Horn	Urban	1 GHz	17	Street
[25]	28 GHz	Rotating Horn	Rotating Horn	Suburban	800 MHz	25	Rooftop
[26]	28,39 GHz	Array	Array	Urban	100 MHz	Continuous	Balcony
[27]	28 GHz	Horn	Horn	Urban	500 MHz	16	Rooftop
[28]	32 GHz	Horn	Horn	Suburban	500 MHz	124	Rooftop
<i>This work</i>	28 GHz	Omni	Rotating Horn	Urban	Narrowband	979	Street, Balcony, Roof

separation between users can help enable algorithm design for Beyond-5G networks [29]–[31].

Using the UMi measurements, we evaluate path loss models with high generalizability. Path loss models are key in determining coverage for Beyond-5G networks, especially for mmWave signals which tend to attenuate rapidly in the presence of blockages (e.g., buildings, foliage, and street clutter). The most common model for UMi mmWave propagation is 3GPP-UMi-NLOS model defined by 3GPP [32], [33]. Another common model is edge diffraction, such as Diffraction-Inspired-NLOS [1]. There are newer models such as Street-Clutter-NLOS [16] and even Over-Top-NLOS [34] for UMa scenarios. The baseline is Slope-Intercept (referred to as Slope-Intercept-NLOS in this paper).

We use the extensive data that we collected and evaluate the NLOS path loss models listed above based on Root Mean Square Errors (RMSE) between the model and data. Using the best path loss model (Street-Clutter-NLOS), we obtain an overall best-fit RMSE of 6.4 dB for UMi propagation, compared to 11.9 dB from the standard 3GPP NLOS model (3GPP-UMi-NLOS). We use Street-Clutter-NLOS to provide NLOS coverage estimates for 90% of users.

The remainder of this paper is organized as follows. Section II discusses related mmWave NLOS measurement campaigns. Section III introduces our measurement campaign. Section IV introduces the path gain models evaluated on the measurements collected. Section V summarizes the results, and Section VI concludes this paper.

## II. RELATED WORK

Previous mmWave NLOS measurement studies were conducted in urban [16]–[24], [26], [27], [35] and suburban environments [25], [28], [36].

These measurement studies used different mmWave or sub-Terahertz (THz) frequencies (e.g., 28/73/142 GHz) and use either directional horn antennas [1], [16], [17], [19], [20], [22], [24], [25], [27], [28] or phased array antennas [18], [26]. Some of these measurement platforms considered in [19] use more complex waveforms and wider bandwidths, but *in general these campaigns lack the scale of measurement provided in this paper*. A summary of related NLOS measurement studies at mmWave and sub-THz is shown in Table I.

Our largest existing NLOS campaign [1] used a rotating horn antenna platform and consists of 120 NLOS links

collected from locations in Lower Manhattan. We use this dataset and 859 links collected in Upper Manhattan to compare path gain models using measurements from Upper and Lower Manhattan, and different BS elevations in the UMi scenario.

## III. MEASUREMENT CAMPAIGN

In this section, we describe our measurement campaign.

### A. Equipment

We use a 28 GHz narrowband channel sounder consisting of a separate transmitter (TX) and receiver (RX) (described in detail in [1], [2]). The omni-directional TX has 0 dBi gain and transmits a +22 dBm continuous-wave tone. The RX is a rotating horn antenna (24 dBi, 14.5 dBi in azimuth, 10 degree 3 dB beamwidth) connected to a mixer that downconverts the received signal to 100 MHz intermediate frequency (IF). The IF signal is recorded by a power meter (20 kHz bandwidth).

### B. Locations

The measurement campaign incorporates two location categories: UMi and UMa. These classifications are important as they correspond to the varied placements of the RX, effectively simulating different BS positions within an urban landscape. At each location, the RX remains stationary, ensuring consistent and controlled data collection. Measurement maps are shown in Fig. 2, and locations are shown in Fig. 3.

In the UMi locations, the BS is positioned *below* the urban clutter, such as nearby buildings. This setup is designed to replicate typical urban scenarios where the BS might be a small cell located on a lightpole or side of a building. The specific UMi measurement locations include **MUD**, **LAW1**, **LAW2**, **CU**, **BN**, and **RIV** (as illustrated in Fig. 3), offering a comprehensive urban coverage model. **7thAVE** is another UMi location which was measured in [1] and is used for comparison later in Section V. Within these UMi sites, the RX deployment varies in elevation. The elevation of the BS is 15–20 m in **MUD**, **LAW1**, **LAW2**, and **7thAVE**. The BS is 1 m high in **CU**, **BN**, and **RIV**.

The UMa locations represent a scenario where the BS is placed *above* the height of neighboring buildings. The elevation of the BS is 50 m above ground in **JLG1** and **JLG2** and about 15 m above neighboring building rooftops.

TABLE II: Summary of the measurement campaign consisting of 20,332,800 NLOS and LOS measurements representing 1,412 links across 35 routes.

Location Type	NLOS (Different Street as BS)			LOS (Same Street as BS)		
	Routes	Measurements	Links	Routes	Measurements	Links
UMi	22	11,980,800	832	13	5,760,000	400
UMa	3	2,116,800	147	2	475,200	33
<b>Total</b>	<b>25</b>	<b>14,097,600</b>	<b>979</b>	<b>15</b>	<b>6,235,200</b>	<b>433</b>

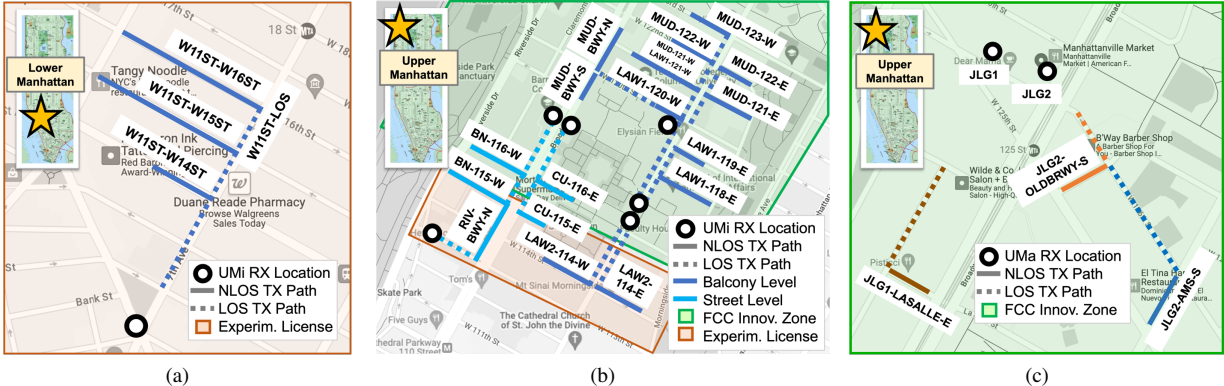


Fig. 2: Maps showing location of RX representing a BS, along with the route of the transmitter representing user equipment. (a-b) are UMi, and (c) is UMa.

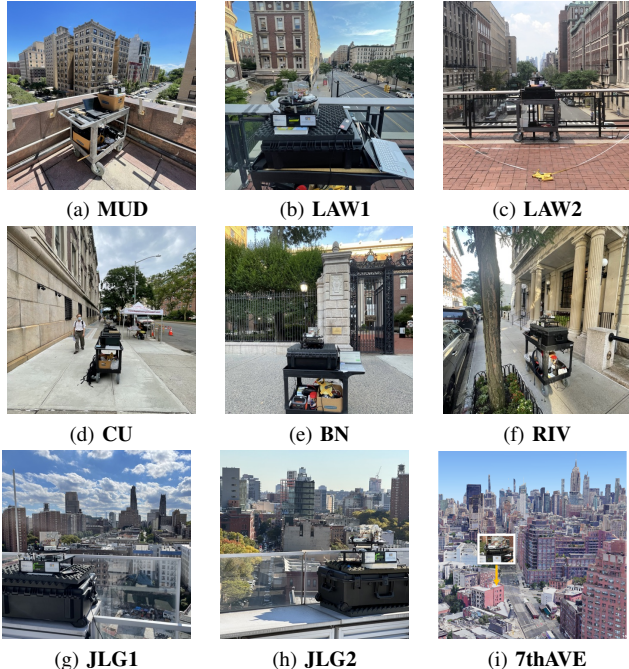


Fig. 3: Representative RX views for each of the seven locations considered. MUD, LAW1, LAW2, and 7thAVE are UMi locations with the BS elevated at 15–20 m. CU, BN, and RIV are UMi locations with the BS elevated at 1 m. JLG1 and JLG2 are UMa locations with the BS elevated at 50 m.

### C. Routes

The TX and RX are both stationary during the measurement (approximately 15,510 power measurements collected for 20 seconds). The RX at each location captures signals from the TX which travels in 1 m intervals away from the RX in a specified route. The TX is stationary during each measurement collection. The TX's route begins with a Before-Corner segment, which represents a UE and BS located on the same street, and transitions into an After-Corner segment to represent a UE and BS located on different streets. This route design is applied to all UMi locations.

For the UMa locations, the campaign contained measurement of 3 NLOS routes and 2 LOS routes. For the UMi locations, this measurement campaign consisted of 22 NLOS routes and 13 LOS routes. The number of routes per scenario is summarized in Table III.

### IV. PATH GAIN MODELS

In this section, we introduce the path gain models used to evaluate the collected measurements. This includes four NLOS models (Street-Clutter-NLOS, Diffraction-Inspired-NLOS, 3GPP-UMi-NLOS, Over-Top-NLOS) and one LOS model (Street-Clutter-LOS). We also use a basic Slope-Intercept-NLOS model for baseline comparisons.

The Street-Clutter-LOS and Street-Clutter-NLOS models we had developed [16] were evaluated using 75 links of measurements collected at one route in Manhattan [16]. The Diffraction-Inspired-NLOS model we had developed [1] was evaluated using 120 links of measurements collected at three routes in Manhattan. 3GPP-UMi-NLOS, an industry standard model for comparison, is discussed in [32], [33]. Finally, our Over-Top-NLOS model was developed in [34].

Unlike the relatively small datasets used for evaluation in [16] and [1], we evaluate Street-Clutter-NLOS, Diffraction-Inspired-NLOS, 3GPP-UMi-NLOS, Over-Top-NLOS, and Street-Clutter-LOS using the extensive measurements we collected, described in Section III.

A detailed description of the models follows below.

#### A. Slope-Intercept-NLOS Model

This is the most commonly used [1]–[3] empirical path loss model which obtains it to parameters, the distance exponent  $n$  and the intercept  $b$  as shown in (1), by fitting to measurement data to minimize fitting error (RMSE) [1]–[3]. In this baseline model (1),  $d_{3D}$  is the 3D Euclidean distance between TX and RX ( $d_{3D}$ ).  $n$  and  $b$  are the distance exponent and intercept of the fitted line.

$$10n \cdot \log_{10} d_{3D} + b, \quad (1)$$

### B. Street-Clutter-LOS Model

The Street-Clutter-LOS model is based on some key parameters: the distance between TX and RX ( $r_1$ ), the signal wavelength ( $\lambda$ ), and an absorption per meter coefficient ( $\kappa_1$ ) [16]. Notably,  $r_1$  denotes the distance between TX and RX *before* the UE travels around a street intersection. The coefficient  $\kappa_1$  quantifies absorption due to average street clutter encountered in the Before-Corner segments. Street-Clutter-LOS path loss is equal to:

$$\left(\frac{\lambda}{4\pi r_1}\right)^2 e^{-\kappa_1 r_1} \quad (2)$$

Here, the path loss  $P_{Street-Clutter-LOS}$  is modeled by considering the free-space path loss ( $\frac{\lambda}{4\pi r_1}$ )<sup>2</sup> and an exponential term that accounts for absorption due to street clutter, characterized by  $\kappa_1$ .

### C. Street-Clutter-NLOS Model

The Street-Clutter-NLOS model assumes that the 28 GHz signal travels through urban canyons, scattering along adjacent buildings [16]. Key parameters include the distances  $r_1$  and  $r_2$  (representing the TX-RX distance before and after turning the corner, respectively), signal wavelength ( $\lambda$ ), absorption coefficients  $\kappa_1$  and  $\kappa_2$  of unit Nep/m, and an effective scattering width of the street intersection  $\sigma_{scat}$ .  $\kappa_1$  is shared with the Street-Clutter-LOS model, while  $\kappa_2$  accounts for absorption in the After-Corner segments. The scattering width,  $\sigma_{scat}$ , is calculated considering the number and width of street poles in the urban environment:

$\sigma_{scat}$  equals  $N_{poles} \times \sigma_{pole}$  where  $N_{poles} = 4$  and  $\sigma_{pole} = 0.24$  m for 4 poles with a width of 0.24 m, typical of NYC.

The Street-Clutter-NLOS path loss is equal to:

$$\frac{\lambda^2 \sigma_{scat}}{(4\pi)^3 r_1 r_2 (r_1 + r_2)} e^{-(\kappa_1 r_1 + \kappa_2 r_2)} \quad (3)$$

This model captures the scattering of the signal as it bends around corners in an urban canyon. The exponential term  $e^{-(\kappa_1 r_1 + \kappa_2 r_2)}$  accounts for the absorption losses before and after the corner. The exponential term and scale factor represents the scattering effects at the corner, influenced by the scattering width  $\sigma_{scat}$ .

### D. Diffraction-Inspired-NLOS Model

The Diffraction-Inspired-NLOS model, as mentioned in the Related Works (Section II) [1], is a diffraction-inspired channel model based on a smaller-scale UMi measurement campaign. Key parameters include distances  $r_1$  and  $r_2$ , and the signal wavelength ( $\lambda$ ). The best fit to data in [1] provided  $n = 2.27$  and  $\alpha = 0.6$  (corresponding to  $-2.2$  dB). Diffraction-Inspired-NLOS path loss is equal to:

$$\frac{\lambda^2}{(4\pi)^2} \left( \left( \frac{1}{r_1 + r_2} \right) \left( \frac{1}{r_1} \right) \left( \frac{1}{r_2} \right) \right)^{n/2} \cdot \alpha \quad (4)$$

In this model, the path loss  $P_{Diffraction-Inspired-NLOS}$  is derived by considering the diffraction effects around corners. The term  $\left( \frac{1}{r_1 + r_2} \right) \left( \frac{1}{r_1} \right) \left( \frac{1}{r_2} \right)$  represents the geometric

spreading and diffraction losses, while the parameter  $\alpha$  captures additional empirical attenuation.

### E. 3GPP-UMi-NLOS Model

The 3GPP-UMi-NLOS model, part of an extensive 5G study conducted by a consortium of universities and companies, offers channel models tailored for mmWave frequencies [32], [33]. The Urban Micro (UMi) scenario, relevant to our study, considers a mobile UE at a height less than 25 m. Key parameters include the 3D Euclidean distance between TX and RX ( $d_{3D}$ ) and the signal wavelength ( $\lambda$ ). A similar model is also provided for UMa scenarios as well.

This model reflects the empirical path loss in urban micro-cell environments. The logarithmic terms account for distance-dependent and frequency-dependent losses, respectively, with coefficients derived from extensive measurements.

### F. Over-Top-NLOS Model

The Over-Top-NLOS model represents a path over the top of clutter, such as buildings [34].

This model assumes that the BS is placed at the rooftop of a building where the antenna elevation is  $z_{BS}$  above surrounding buildings of height  $z_c$ . The UE is assumed to be placed at an elevation of  $z_m$  from the ground. Ground reflection is represented with coefficient  $\Gamma_g$ .  $T_{eff}$  is the effective power transmission coefficient through the exterior wall. This model integrates the effects of diffraction and reflection over the building tops, capturing the additional losses due to the elevated path. Over-Top-NLOS path loss is equal to:

$$\frac{\lambda^2 (z_{BS} - z_c)^2 e^{-\kappa|z_c - z_m|} |\Gamma_g|^2}{8\pi^2 r^4} \quad (5)$$

In this model, the path loss  $P_{Over-Top-NLOS}$  is influenced by the elevation difference ( $z_{BS} - z_c$ ), which determines the diffraction losses over buildings. The term  $e^{-\kappa|z_c - z_m|}$  accounts for the additional absorption through the clutter, while the factor  $|\Gamma_g|^2$  incorporates the transmission and reflection effects at the ground.

## V. MEASUREMENT RESULTS

In this section, we begin by comparing path loss models with the collected data. We also examine the AoA of the received signals to help assess the use of beam tracking and MU-MIMO in Beyond-5G networks.

### A. Path Gain Model-Data Comparison

In the UMi evaluation, we compare the models Slope-Intercept-NLOS, Street-Clutter-NLOS, Diffraction-Inspired-NLOS, and 3GPP-UMi-NLOS to the UMi After-Corner measurements collected. For the Before-Corner measurements collected, we check how well they correspond with the Street-Clutter-LOS model. In the UMa evaluation, we compare the fit of the Over-Top-NLOS and Street-Clutter-NLOS models to the UMa After-Corner measurements.

**Comparing UMi Path Gain Models** Our analysis shows that the Street-Clutter-NLOS, Diffraction-Inspired-NLOS, and

Street-Clutter-LOS models, as detailed in Section IV, align well with the measurements taken in the UMi scenarios. These models demonstrate reasonable accuracy, with an average RMSE of 6.4, 6.6, and 6.4 dB, respectively, for all the measured UMi After-Corner routes in Upper and Lower Manhattan. This level of accuracy indicates a reliable performance in modeling the signal behavior in these specific urban settings. However, it is observed that the Slope-Intercept-NLOS and 3GPP-UMi-NLOS models exhibit a slightly lower accuracy, with an average RMSE of 8.2 and 11.9 dB, respectively, suggesting a less precise fit for the same measurement set. For a detailed comparison, the RMSE values for individual routes are provided in Table III.

**Comparing Two Parts of Manhattan With Street-Clutter-NLOS Model** Our measurement campaign, as outlined in Section III, extensively measures regions within the FCC Innovation Zone area in Upper Manhattan, including locations labeled as **MUD**, **LAW1**, **LAW2**, **CU**, **BN**, and **RIV**. Additionally, we include a smaller set of measurements from Lower Manhattan (**7thAVE**), characterized by slightly different building geometries. We aim to compare the Street-Clutter-NLOS and Street-Clutter-LOS models in these two regions.

It is important to recall that both Street-Clutter-NLOS and Street-Clutter-LOS models share the  $\kappa_1$  parameter, representing the average scattering due to street clutter in the Before-Corner segments. Considering the consistent presence of foliage across streets, we set the  $\kappa_2$  parameter in the Street-Clutter-NLOS model, responsible for the After-Corner segments, equal to  $\kappa_1$ . For clarity, we refer to these collectively as  $\kappa$ . In our analysis, detailed in Table III, we use 0.019 dB/m.

When adjusting  $\kappa$  specifically for the Upper Manhattan measurements in Fig. 2(b), a  $\kappa$  of 0.029 dB/m offers the best fit resulting in RMSEs of 5.8 and 5.6 dB for the Street-Clutter-NLOS and Street-Clutter-LOS models, respectively. For Lower Manhattan measurements in Fig. 2(c), a value of 0.000 dB/m yields the most accurate results for the Street-Clutter-NLOS and Street-Clutter-LOS models, with RMSEs of 8.6 and 9.3 dB, respectively. This suggests that the average scattering due to street clutter is significantly different between these two parts of Manhattan. We note that Upper Manhattan measurement locations tended to be narrower with more street clutter the signal could scatter off of (e.g., foliage, buildings, cars, lightpoles, etc.). Lower Manhattan measurement locations tended to have wider street areas, more skyscrapers, less foliage, and less general street clutter for the given area.

**Comparing Balcony vs. Street Level With Street-Clutter-NLOS Model** In our measurement campaign, we collected several UMi measurements at two different elevations: Balcony Level and Street Level. This part of the study focuses on comparing the accuracy of the Street-Clutter-NLOS and Street-Clutter-LOS models based on these varying elevation measurements, in hopes of better understanding how the change in RX elevation impacts UMi propagation.

When adjusting the absorption parameter  $\kappa$  for the Balcony Level measurements, we find that a  $\kappa$  value of 0.028 dB/m offers the most accurate fit for both the Street-Clutter-NLOS and

Street-Clutter-LOS models. The resulting RMSEs for these models are 6.1 and 6.2 dB, respectively. This demonstrates a relatively high level of accuracy at the Balcony Level.

In contrast, for measurements taken at Street Level, the optimal  $\kappa$  value increases to 0.044 dB/m. With this adjustment, the best fit for the Street-Clutter-NLOS and Street-Clutter-LOS models results in RMSEs of 4.4 and 4.4 dB, respectively. The need for a higher  $\kappa$  value at Street Level is consistent with our expectations. At a lower elevation, the RX faces more direct obstructions, such as trees and cars, which are less prevalent at the higher Balcony Level. This increased obstruction at Street Level naturally leads to a higher absorption parameter, reflecting the impact on signal propagation.

These observations underscore the importance of considering the urban landscape's vertical dimension when developing and tuning propagation models for UMi scenarios, where the elevation of the BS could impact the amount of immediate obstructions faced by the mmWave signal, and as a result, the Beyond-5G network coverage.

**Foliage Density Analysis** We build a linear model correlating the foliage density in measured Before-Corner and After-Corner segments with the absorption parameter  $\kappa$ , as utilized in the Street-Clutter-LOS and Street-Clutter-NLOS models (refer to Section IV). This model would aid in quantifying the impact of urban foliage on mmWave signal absorption.

A primary challenge in this analysis is the accurate assessment of foliage density for each street segment. To address this, we utilize the NYC Tree Map database, a comprehensive resource that catalogs every tree in New York City [37]. We manually tally the number of trees present in each segment under consideration. We define the Before-Corner segment as the area between the RX and the furthest street intersection where the TX turned the corner. We define the After-Corner segment as the area between where one enters the corner and the furthest the TX was able to travel. We calculate the area of these segments, and through this analysis, we establish if a clear relationship between foliage density and the  $\kappa$  absorption parameter exists.

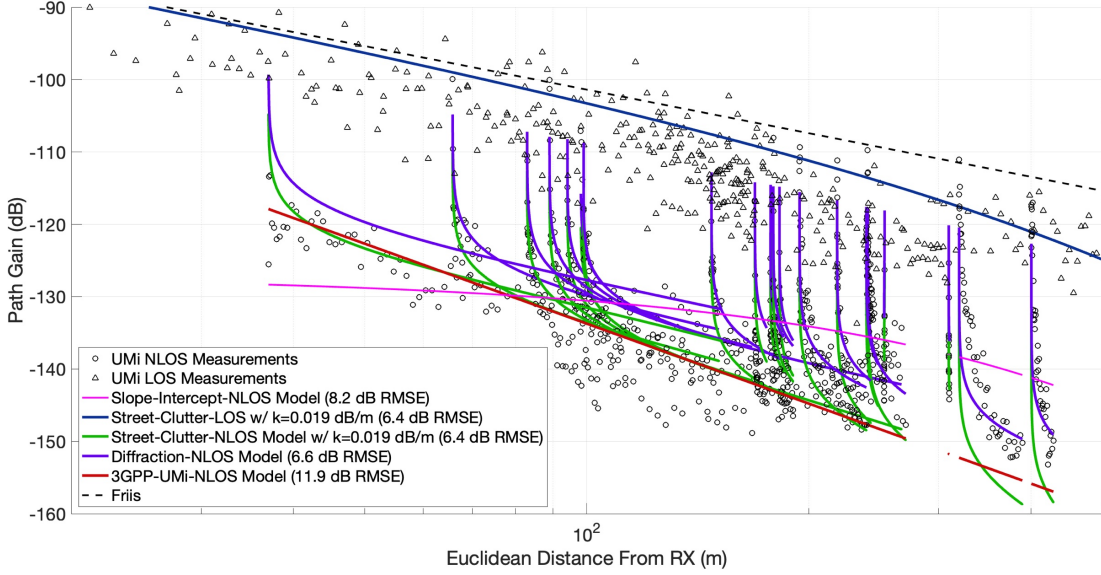
For each Before-Corner dataset, we find the optimal  $\kappa_1$  by fitting. We use the foliage densities for Before-Corner street segments to create a linear fit which maps foliage density to  $\kappa_1$ . We perform a similar approach for the After-Corner street segments and their respective foliage density values. We find the optimal  $\kappa_2$  for each dataset by fitting. We create a linear fit which maps After-Corner foliage density values to  $\kappa_2$ .

The result is a more optimized version of the Street-Clutter-NLOS model with  $\kappa_1$  and  $\kappa_2$  determined by foliage density. This model performs 0.1 dB better than the Street-Clutter-NLOS model with 6.3 dB RMSE, which is a negligible improvement. This indicates a limited relationship between foliage and  $\kappa$  (recall that  $\kappa$  accounts for scattering from lightpoles and street clutter, not just foliage). More complex models have shown to provide a relationship between path loss and foliage [34]. The detailed RMSE per UMi dataset is shown in Table III.

#### K-Folds Cross Validation on UMi Balcony Level Data

TABLE III: NLOS models evaluated on Upper and Lower Manhattan UMi measurements.

Dataset	Best-Fit RMSE of UMi NLOS Models (dB)				
	Slope-Intercept-NLOS	$\kappa$	$\epsilon$	3GPP-UMi-NLOS	Foliage $\kappa=f(foliage)$
Parameters	$b,n$	$\kappa$	$\epsilon$	N/A	$\kappa=f(foliage)$
7thAVE-W14ST	8.9	11.5	6.3	20.0	10.9
7thAVE-W15ST	11.4	15.0	9.1	19.3	13.6
7thAVE-W16ST	12.1	17.0	10.0	22.7	16.0
MUD-122-E	6.9	2.7	5.5	10.8	3.0
MUD-121-E	9.8	5.3	8.3	8.1	6.2
MUD-121-W-19	7.8	5.0	4.0	7.1	4.0
MUD-121-W	5.2	4.5	5.7	6.6	4.2
MUD-122-W	5.9	4.1	8.6	8.1	4.4
MUD-123-W	5.5	4.3	10.2	11.1	4.5
LAW1-118-E	8.6	3.0	4.4	6.6	3.4
LAW1-119-E	6.0	3.3	3.6	9.8	2.9
MUD-BWY-N	10.4	9.3	5.1	18.5	8.8
MUD-BWY-S	9.0	10.6	5.3	20.4	10.1
LAW1-120-W	9.0	7.6	3.5	16.7	7.1
LAW1-121-W	4.8	1.7	6.7	14.6	1.7
LAW2-114-E	9.9	8.9	5.6	14.6	8.3
LAW2-114-W	8.4	3.2	3.9	8.7	2.9
BN-116-W	9.3	4.4	5.5	8.7	4.9
BN-115-W	8.2	3.8	6.8	9.8	4.2
CU-116-E	8.5	5.0	8.1	7.9	5.6
CU-115-E	8.5	6.0	10.2	9.2	6.3
RIV-BWY-N	7.0	5.0	8.2	3.1	5.9
Average:	8.2	6.4	6.6	11.9	6.3


 Fig. 4: Measured path gain for UMi scenario using measurements from Upper and Lower Manhattan. Fitted lines for Slope-Intercept-NLOS, Street-Clutter-NLOS, Diffraction-Inspired-NLOS, 3GPP-UMi-NLOS, and Street-Clutter-LOS models are included as well as  $\kappa$  value.

K-Folds Cross Validation is a method where we test on one unseen dataset and do so for all options/folds of what the unseen dataset could be (K-Folds, or 5-Folds in this case). In this method, the first step is Algorithm 1. We first initialize the  $k_{sweep}$  array. It spans from 0 to 0.06 with 60 increments, representing different  $\kappa$  values between 0.000 and 0.060 with precision of 0.001. For each  $\kappa$  value, we load the relevant dataset and compute the path loss and RMSE for both NLOS and LOS scenarios. These RMSE values are then stored and plotted against the  $k_{sweep}$  array to identify the optimal  $\kappa$  value, also referred to as  $k_{trained}$ .

As visualized in Table IV, the second step is to now infer path loss for unseen data. We select 5 MUD datasets, in

which 4 will be used for training and 1 will be used for inference. Choosing one dataset to infer path loss for gives us five combinations/splits to compute RMSE and determine the average RMSE across all 5 splits. Average RMSE across 5 training/inference splits of the data is 5.1 dB for the NLOS case and 5.2 dB for the LOS case.

In the final step shown in Fig. 5, we verify the path loss predictions from Table IV by training  $\kappa$  from all 5 MUD datasets. After doing so, the optimal  $\kappa$  is 0.048 dB/m with an RMSE of 5.1 dB. This agrees with the 5.2 and 5.1 LOS/NLOS Average Inference RMSE estimated through K-Folds Cross Validation (Table IV).

**UMa Path Gain Models** We find that the Over-Top-NLOS

**Algorithm 1** Sweep  $\kappa$  to optimize NLOS/LOS models

```

1:  $k\_sweep \leftarrow \text{linspace}(0, 0.06, 60)$ 
2: for  $i = 1$  to  $\text{length}(k\_sweep)$  do
3:    $k\_under\_test \leftarrow k\_sweep[i]$ 
4:   Load data from files
5:   Compute distances and measured path losses
6:   if NLOS then
7:     Compute theoretical path loss for NLOS using  $k\_under\_test$ 
8:     Compute RMSE for NLOS (measurement vs. theoretical)
9:   else
10:    Compute theoretical path loss for LOS using  $k\_under\_test$ 
11:    Compute RMSE for LOS (measurement vs. theoretical)
12:  end if
13:  Store RMSE values
14: end for
15: Plot RMSE values against  $k\_sweep$ 
16: Identify and plot the optimal kappa value
17: Set  $k\_trained \leftarrow$  optimal kappa value

```

TABLE IV: Evaluate trained NLOS/LOS model on unseen data.

Data	Split 1	Split 2	Split 3	Split 4	Split 5
MUD-123-W	Train	Train	Train	Train	Infer
MUD-122-W	Train	Train	Train	Infer	Train
MUD-121-W	Train	Train	Infer	Train	Train
MUD-121-E	Train	Infer	Train	Train	Train
MUD-122-E	Infer	Train	Train	Train	Train
<b>Per-Split Inference RMSE (dB)</b>					
Street-Clutter-LOS	2.4	4.1	7.3	5.9	6.3
Street-Clutter-NLOS	7.7	3.8	7.2	3.2	3.5
<b>Street-Clutter-LOS Average Inference RMSE (dB)</b>					
	5.2				
<b>Street-Clutter-NLOS Average Inference RMSE (dB)</b>					
	5.1				

model is consistent with the UMa measurements collected. This model achieves an average RMSE of 4.3 dB across all UMa NLOS routes measured, which is 6.6 dB more accurate than the Street-Clutter-NLOS model. Recall that the Street-Clutter-NLOS model assumes that the mmWave signal primarily follows the urban canyon from the base, turning the corner to reach the mobile. The Over-Top-NLOS model assumes that the mmWave signal primarily propagates directly over the tops of buildings separating the rooftop base from the mobile. Over-Top-NLOS and Street-Clutter-NLOS model comparisons to UMa data are illustrated in Fig. 6, as well as Slope-Intercept-NLOS and 3GPP-UMa-NLOS which perform equally well as Over-Top-NLOS.

### B. AoA Evaluation

We inspect the AoA of the signals received in both UMi and UMa scenarios. We want to see if the 28 GHz signals arrive directly from the TX to the RX (geometric direct shot) or if they take a different path, such as through the urban canyon. We do this by quantifying its fit/divergence from the geometric direct shot path between TX and RX.

1) **UMa AoA:** We analyzed the AoA of the transmitted signal by identifying the angle of highest received power from the rotating RX. Detailed AoA results for each UMa location are shown in Fig. 7 and Table VI. We plotted the AoA from consecutive measurements of both Before-Corner and After-Corner segments in blue and orange, respectively, along with the geometric direct shot AoA.

For Before-Corner segments, the average error compared to the geometric direct shot is 2.0 degrees (standard deviation

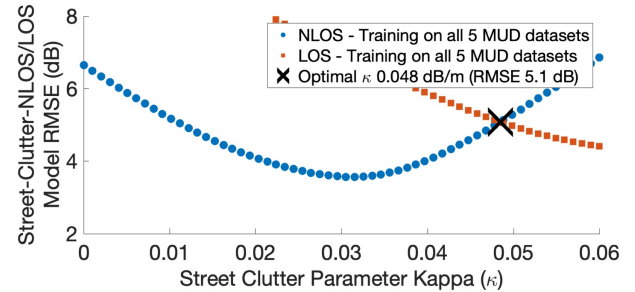


Fig. 5: We verify the path loss predictions from Table IV by training  $\kappa$  from all 5 MUD datasets.

TABLE V: Path loss modeling for the UMa scenario. Over-Top-NLOS appears to be the dominant propagation mechanism, with a 7 dB improvement compared to Street-Clutter-NLOS.

JLG Best-Fit RMSE of UMa NLOS Models (dB)				
Model	LASALLE	OLDBRWY	AMS	Avg.
Slope-Intercept-NLOS	3.3	3.6	4.9	3.9
Street-Clutter-NLOS	8.3	11.0	14.0	11.1
Street-Clutter-NLOS + Over-Top-NLOS	3.4	5.2	3.6	4.1
Over-Top-NLOS	3.3	5.1	4.4	4.3
3GPP-UMa-NLOS	3.1	3.6	7.0	4.6

9.5 degrees). For After-Corner segments, the average error is 3.5 degrees (standard deviation 18.5 degrees).

**JLG1** The recorded peak angle aligns with the geometric direct shot, especially in the After-Corner segment. The average bias for the After-Corner segment is 5.7 degrees, with a large standard deviation of 27.2 degrees, where some error from reflections with AoA approximately 180 degrees away, likely indicating reflections from large buildings behind the RX. Given **JLG1**'s rooftop location, 20 m higher than nearby buildings, such signal propagation over the top of buildings is reasonable.

**JLG2** Similar to **JLG1**, the recorded peak angle aligns with the geometric direct shot, especially in the After-Corner segments. The average bias for closer and further After-Corner segments are 0.3 and 4.4 degrees, respectively with standard deviation around 14 degrees for both cases. Some reflections with AoA approximately 180 degrees away likely indicate reflections from large buildings behind the RX. Given **JLG2**'s rooftop location, 20 m higher than nearby buildings, such propagation is reasonable to observe.

2) **UMi AoA:** We analyzed the AoA of the transmitted signal by identifying the angle of highest received power using a rotating RX collecting power measurements at 360 degrees with 1 degree intervals. Detailed results for each UMi location are shown in Fig. 8 and Table VII, including consecutive measurements for both Before-Corner and After-Corner segments, plotted in blue and orange, respectively, along with the geometric direct shot AoA.

For Before-Corner segments, the average error compared to the geometric direct shot is 3.1 degrees (standard deviation 10.1 degrees). For After-Corner segments, the average error is 18.5 degrees (standard deviation 16.8 degrees). These findings improve our understanding of urban mmWave signal propagation in the UMi scenario, particularly when both the BS and

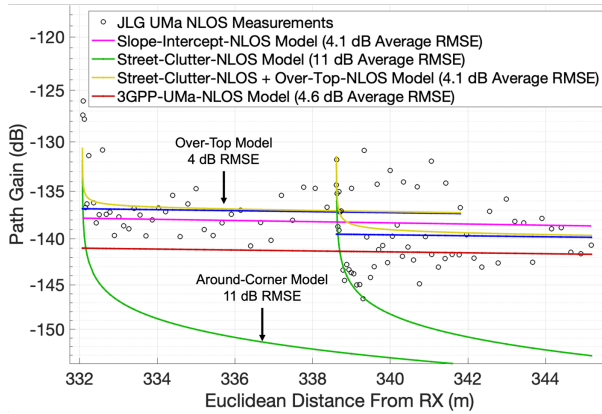


Fig. 6: Measured path gain values for the UMa scenario and their fitted lines for the Over-Top-NLOS and Street-Clutter-NLOS models.

TABLE VI: AoA error vs. TX/RX direction of UMa locations.

Dataset	RX Peak Angle vs. TX/RX Direction (deg)			
	$\mu$ NLOS	$\sigma$ NLOS	$\mu$ LOS	$\sigma$ LOS
JLG1-LASALLE	5.7	27.2	0.1	21.0
JLG2-OLD-BWY	0.3	14.5	3.0	3.7
JLG2-AMS	4.4	14.0	3.0	3.7
<b>Average:</b>	3.5	18.5	2.0	9.5

UE are below neighboring buildings' elevation.

**7thAVE** The peak AoA aligns with the geometric direct shot, especially around 400 m, indicating the signal mainly propagates through the street canyon, with multipath scattering and reflections from nearby buildings before reaching the RX.

**MUD** The peak signal angle aligns with the urban canyon's orientation. During the initial phase (50-100 m), the AoA converges to this angle, likely due to the slight offset of the RX and TX, with the TX about 10-20 m away from the RX.

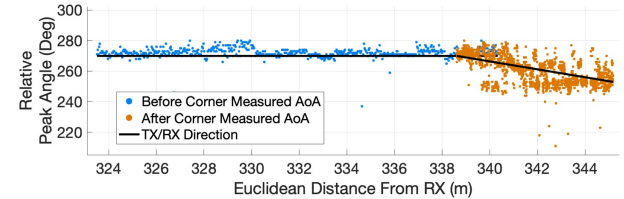
**LAW1 and LAW2** These T-intersection locations show peak signal angles scattering from the building opposite the After-Corner direction, especially near 100-200 m, indicating pronounced signal reflection and scattering.

**BN** The peak angle predominantly aligns with the urban canyon direction near 270 degrees. Between 100-150 m, signals arrive primarily from 250 degrees, possibly reflecting off trees or buildings. Trees along Broadway may act as reflectors.

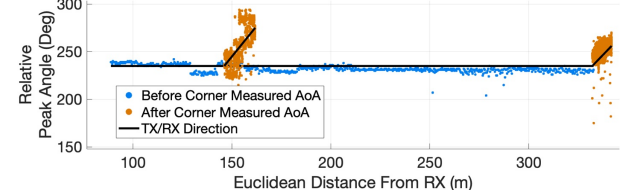
**CU** The After-Corner measurements near 75-100 m at a campus entrance show scattering from the urban canyon at around 270 degrees and from reflectors at about 310 degrees, likely due to trees along Broadway. The 175 m measurements occur at a conventional intersection.

**RIV** The peak angle of the received signal consistently aligns with the urban canyon direction, near 270 m.

In summary, our AoA analysis across datasets indicates that the primary propagation path in UMi scenarios is predominantly through the urban canyon. The Before-Corner segment closely aligns with the geometric direct shot path, while the After-Corner segment diverges gradually. From the BS perspective, most After-Corner links have the same AoA as the last LOS link at the corner, indicating scattering/diffraction at the corner as the dominant propagation path. Generally, in traditional four-way intersections, the strongest mmWave signal component tends to follow the urban canyon path rather



(g) JLG1



(h) JLG2

Fig. 7: Relative AoA vs. TX/RX Direction for all UMa measurement locations.

TABLE VII: AoA error vs. TX/RX direction of UMi locations.

Dataset	RX Peak Angle vs. TX/RX Direction (deg)			
	$\mu$ NLOS	$\sigma$ NLOS	$\mu$ LOS	$\sigma$ LOS
7thAVE-W14ST	13.4	10.3	1.4	7.3
7thAVE-W15ST	11.8	21.7	1.4	7.3
7thAVE-W16ST	10.0	22.6	1.4	7.3
MUD-122-E	9.4	8.1	5.0	4.1
MUD-121-E	14.9	11.8	7.9	8.9
MUD-121-W-19	4.6	40.7	5.5	14.4
MUD-121-W	30.0	19.0	5.5	14.4
MUD-122-W	20.8	13.2	8.7	8.0
MUD-123-W	12.7	10.0	2.3	3.3
LAW1-118-E	44.2	29.2	3.6	14.2
LAW1-119-E	31.0	14.7	5.1	14.3
MUD-BWY-N	12.7	10.0	0.1	13.3
MUD-BWY-S	14.4	15.7	N/A	N/A
LAW1-120-W	21.9	11.4	0.2	7.6
LAW1-121-W	15.2	10.1	1.0	4.7
LAW2-114-E	25.6	13.4	N/A	N/A
LAW2-114-W	18.0	17.4	N/A	N/A
BN-116-W	20.6	18.0	3.6	40.9
BN-115-W	14.3	11.7	1.7	5.8
CU-116-E	25.8	23.0	2.5	5.6
CU-115-E	6.4	17.3	0.8	7.8
RIV-BWY-N	28.7	19.2	1.0	3.5
<b>Average:</b>	18.5	16.8	3.1	10.1

than scattering over nearby buildings.

### C. Data Rate Estimates

This section provides initial estimates of data rates expected at street intersections, relevant for mmWave Fixed Wireless Access (FWA) such as LinkNYC in NYC [38]. A LinkNYC mmWave FWA deployment at Amsterdam Ave. and 118th St. overlaps with the **LAW1-118-E** corner location.

A key question for wireless network service providers is the deployment density required to ensure adequate coverage. While these measurements may not cover every possible real-world scenario, they provide an initial expectation.

According to the Street-Clutter-NLOS model, path gain depends on  $r_1$  (pre-corner distance) and  $r_2$  (post-corner distance). The Before-Corner distance is assumed to be either 100 m or 200 m, representing deployments at every one or two intersections, respectively, based on average NYC block dimensions.

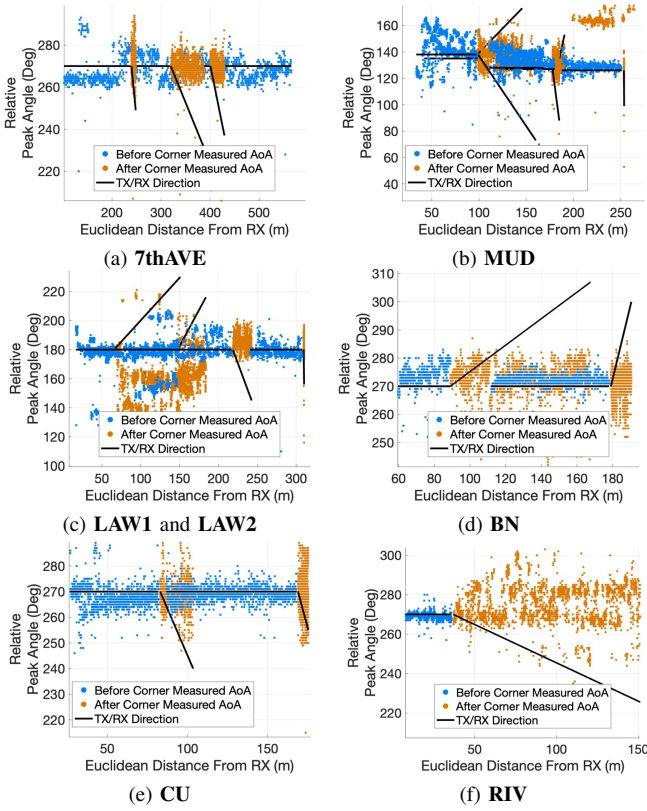


Fig. 8: Relative AoA vs. TX/RX Direction for all UMi measurement locations.

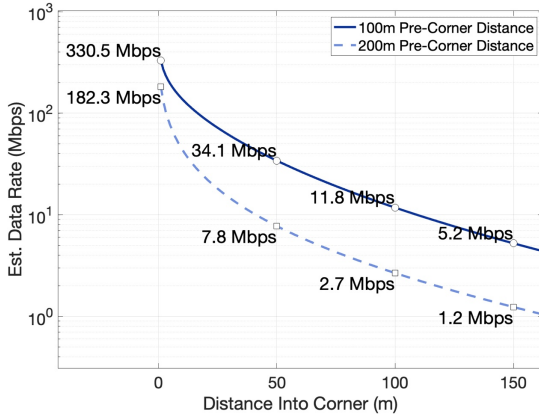


Fig. 9: Data rate estimates for 100m and 200m pre-corner distances.

We assume a 100 MHz bandwidth for mmWave FWA. The degradation in gain ( $G_{deg}$ ) is calculated using a two-step process: first, determining the effective beamforming gain from After-Corner measurements for 90% coverage, then calculating the difference from the nominal 14.5 dB gain. The path gain ( $G_{path}$ ) is derived using  $\kappa_1 = \kappa_2 = 0.019$  dB/m, optimal for Upper and Lower Manhattan.  $r_1$  is either 100 m or 200 m, with  $r_2$  being the variable of interest.

To estimate SNR and data rate, we use the following parameters: 100 MHz bandwidth, 9 dBi receiver gain, 9 dB receiver noise figure, and -85 dBm noise floor. The transmitter power is 28 dBm, with gain of 23 dBi and, respectively. We also consider a shadow fading margin (SFM) of 7.5 dB which

is a function of Street-Clutter-NLOS best-fit RMSE.

The SNR is calculated using the equation:

$$SNR = P_{TX} + G_{TX} + G_{RX} - G_{deg} - G_{path} - SFM - NF_{RX}$$

Including an overhead factor ( $\rho$ ) of 0.6 and an implementation penalty ( $IP$ ) of 3 dB, the data rate is determined by:

$$Rate_{data} = \rho B \log_2 \left( 1 + 10^{\frac{SNR - IP}{10}} \right)$$

These calculations provide a preliminary understanding of data rates in urban mmWave settings. However, future work should incorporate factors like modulation, channel coding, and MAC resource scheduling to refine these estimates. Fig. 9 presents data rate estimates for 100m and 200m Before-Corner distances. As can be seen in the figure, even with 100m separation between deployments, the estimated data rate drops from 330 Mbps to 34 Mbps after traveling just 50 m into the corner. The average length of a NYC block is over 150 m, and at 150 m, the data rate drops by a factor of over 60 times compared to entering the corner.

## VI. CONCLUSION

This study conducted extensive mmWave measurements in the COSMOS FCC Innovation Zone in Manhattan, resulting in over 20 million data points to evaluate path loss models.

The results in this paper show that our Diffraction-Inspired-NLOS and Street-Clutter-NLOS models outperform the standard 3GPP-UMi-NLOS model by over 5 dB. Our Over-Top-NLOS model also performs well with an RMSE of 4.3 dB, suggesting its viability for elevated deployments.

Key insights include the impact of foliage and street clutter on path loss, with higher path loss associated with higher foliage density. Base station height is crucial, with lower heights experiencing more signal attenuation. Analysis of AoA indicates potential for MU-MIMO when in UMa scenarios.

These findings provide insights for Beyond-5G mmWave networks, emphasizing the importance of environmental factors and specific deployment scenarios. In particular, MU-MIMO may be feasible over rooftops, but is limited at balcony levels common in urban deployments. Where such rooftops are available, the dominant angle of arrival (AoA) deviates by only 2 to 3.5 degrees from the direct transmitter/receiver direction. This small deviation allows for effective spatial separation between users, facilitating the future development of MU-MIMO algorithms for Beyond-5G networks. For UMi scenarios, we offer reliable around-corner coverage estimates through extensive measurements.

## VII. ACKNOWLEDGEMENTS

This work was supported by NSF grants CNS-1827923, OAC-2029295, EEC-2133516, AST-2232455, CNS-2148128; and in part by the Funds from Federal Agency and Industry Partners as specified in the NSF Resilient and Intelligent NextG Systems (RINGS) Program. Rodolfo Feick's work is supported by Chilean Research Agency grants PIA/APOYO AFB180002 and ANID/REDES 180144. We thank Aditya Jolly for his help in taking measurements and Prof. Tingjun Chen for his helpful suggestions.

## REFERENCES

- [1] J. Du, D. Chizhik, R. A. Valenzuela, R. Feick, G. Castro, M. Rodriguez, T. Chen, M. Kohli, and G. Zussman, "Directional Measurements in Urban Street Canyons From Macro Rooftop Sites at 28 GHz for 90% Outdoor Coverage," *IEEE Trans. Antennas Propag.*, vol. 69, no. 6, pp. 3459–3469, 2021.
- [2] T. Chen, M. Kohli, T. Dai, A. Estigarribia, D. Chizhik, J. Du, R. Feick, R. Valenzuela, and G. Zussman, "28 GHz Channel Measurements in the COSMOS Testbed Deployment Area," in *Proc. of ACM mmNets'19*, 2019.
- [3] M. Kohli, A. Adhikari, G. Avci, S. Brent, J. Moser, S. Hossain, A. Dash, I. Kadota, R. Feick, D. Chizhik, J. Du, R. Valenzuela, and G. Zussman, "Outdoor-to-Indoor 28 GHz Wireless Measurements in Manhattan: Path Loss, Location Impacts, and 90% Coverage," in *Proc. of ACM MobiHoc'22*, 2022.
- [4] D. Chizhik, J. Du, R. Feick, M. Rodriguez, G. Castro, and R. Valenzuela, "Path Loss and Directional Gain Measurements at 28 GHz for Non-Line-of-Sight Coverage of Indoors With Corridors," *IEEE Trans. Antennas Propag.*, vol. 68, no. 6, pp. 4820–4830, 2020.
- [5] V. Raghavan, A. Partyka, and A. Sampath et al., "Millimeter-Wave MIMO Prototype: Measurements and Experimental Results," *IEEE Commun. Mag.*, vol. 56, no. 1, pp. 202–209, 2018.
- [6] K. Du, O. Ozdemir, F. Erden, and I. Guvenc, "28 GHz Indoor and Outdoor Propagation Measurements and Analysis at a Regional Airport," in *Proc. of IEEE PIMRC'21*, 2021.
- [7] S. Jun, D. Caudill, J. Chuang, P. Papazian, A. Bodí, C. Gentile, J. Senic, and N. Golmie, "Penetration Loss at 60 GHz for Indoor-to-Indoor and Outdoor-to-Indoor Mobile Scenarios," in *Proc. of European Conference on Antennas and Propagation (EuCAP)'20*, 2020.
- [8] H. Zhao, R. Mayzus, S. Sun, M. Samimi, J. Schulz, Y. Azar, K. Wang, G. Wong, F. Gutierrez, and T. Rappaport, "28 GHz Millimeter Wave Cellular Communication Measurements for Reflection and Penetration Loss In and Around Buildings in New York City," in *Proc. of IEEE ICC'13*, 2013.
- [9] M. Aslam, Y. Corre, J. Belschner, G. Arockiaraj, and M. Jäger, "Analysis of 60-GHz In-street Backhaul Channel Measurements and LiDAR Ray-based Simulations," in *Proc. of European Conference on Antennas and Propagation (EuCAP)'20*, 2020.
- [10] J. Du, D. Chizhik, R. Feick, M. Rodríguez, G. Castro, and R. Valenzuela, "Suburban Fixed Wireless Access Channel Measurements and Models at 28 GHz for 90% Outdoor Coverage," *IEEE Trans. Antennas Propag.*, vol. 68, no. 1, pp. 411–420, 2020.
- [11] C. Diakhate, J. Conrat, J. Cousin, and A. Sibille, "Millimeter-wave Outdoor-to-Indoor Channel Measurements at 3, 10, 17 and 60 GHz," in *Proc. of European Conference on Antennas and Propagation (EuCAP)'17*, 2017.
- [12] C. Bas, R. Wang, T. Choi, S. Hur, K. Whang, J. Park, J. Zhang, and A. F. Molisch, "Outdoor to Indoor Penetration Loss at 28 GHz for Fixed Wireless Access," in *Proc. of IEEE ICC'18*, 2018.
- [13] C. Larsson, F. Harrysson, B. Olsson, and J. Berg, "An Outdoor-to-Indoor Propagation Scenario at 28 GHz," in *Proc. of European Conference on Antennas and Propagation (EuCAP)'14*, 2014.
- [14] I. Khan, M. Ghoshal, S. Aggarwal, D. Koutsonikolas, and J. Widmer, "Multipath TCP in Smartphones Equipped with Millimeter Wave Radios," in *Proc. of ACM WiNTECH'21*, 2021.
- [15] D. Raychaudhuri, I. Seskar, G. Zussman, T. Korakis, D. Kilper, T. Chen, J. Kolodziejski, M. Sherman, Z. Kostic, X. Gu, H. Krishnaswamy, S. Moshwari, P. Skrimponis, and C. Guterman, "Challenge: COSMOS: A City-Scale Programmable Testbed for Experimentation with Advanced Wireless," in *Proc. of ACM MobiCom'20*, 2020.
- [16] D. Chizhik, J. Du, M. Kohli, A. Adhikari, R. Feick, R. Valenzuela, and G. Zussman, "Accurate Urban Path Loss Models Including Diffuse Scatter," in *Proc. of European Conference on Antennas and Propagation (EuCAP)'23*, 2023.
- [17] T. S. Rappaport, G. MacCartney, S. Sun, H. Yan, and S. Deng, "Small-Scale, Local Area, and Transitional Millimeter Wave Propagation for 5G Communications," *IEEE Trans. Antennas Propag.*, vol. 65, no. 12, pp. 6474–6490, 2017.
- [18] R. Wang, C. U. Bas, S. Sangodoyin, S. Hur, J. Park, J. Zhang, and A. F. Molisch, "Stationarity Region of mmWave Channel Based on Outdoor Microcellular Measurements at 28 GHz," in *Proc. of IEEE MILCOM'17*, 2017.
- [19] J. Ko, Y. Cho, S. Hur, T. Kim, J. Park, A. F. Molisch, K. Haneda, M. Peter, D. Park, and D. Cho, "Millimeter-Wave Channel Measurements and Analysis for Statistical Spatial Channel Model in In-Building and Urban Environments at 28 GHz," *IEEE Trans. Wirel. Commun.*, vol. 16, no. 9, pp. 5853–5868, 2017.
- [20] T. S. Rappaport, S. Sun, R. Mayzus, H. Zhao, Y. Azar, K. Wang, G. N. Wong, J. K. Schulz, M. Samimi, and F. Gutierrez, "Millimeter Wave Mobile Communications for 5G Cellular: It Will Work!" *IEEE Access*, vol. 1, pp. 335–349, 2013.
- [21] Y. Xing and T. S. Rappaport, "Millimeter Wave and Terahertz Urban Microcell Propagation Measurements and Models," *IEEE Commun. Lett.*, vol. 25, no. 12, pp. 3755–3759, 2021.
- [22] T. S. Rappaport, G. R. MacCartney, M. K. Samimi, and S. Sun, "Wideband Millimeter-Wave Propagation Measurements and Channel Models for Future Wireless Communication System Design," *IEEE Trans. Commun.*, vol. 63, no. 9, pp. 3029–3056, 2015.
- [23] T. S. Rappaport, E. Ben-Dor, J. N. Murdock, and Y. Qiao, "38 GHz and 60 GHz Angle-Dependent Propagation for Cellular Peer-to-Peer Wireless Communications," in *Proc. of IEEE ICC'12*, 2012.
- [24] S. Ju and T. S. Rappaport, "140 GHz Urban Microcell Propagation Measurements for Spatial Consistency Modeling," in *Proc. of IEEE ICC'21*, 2021.
- [25] Y. Zhang, S. Jyoti, C. Anderson, D. Love, N. Michelusi, A. Sprintson, and J. Krogmeier, "28 GHz Channel Measurements and Modeling for Suburban Environments," in *Proc. of IEEE ICC'18*, 2018.
- [26] A. Narayanan, M. I. Rochman, A. Hassan, B. S. Firmansyah, V. Sathya, M. Ghosh, F. Qian, and Z. Zhang, "A Comparative Measurement Study of Commercial 5G mmWave Deployments," in *Proc. of IEEE INFOCOM'22*, 2022.
- [27] K. Kim, M. Kim, J. Park, J. Lee, J. Liang, and K. Lee, "Diffraction Loss Model Based on 28 GHz Over-Rooftop Propagation Measurements," in *Proc. of IEEE Vehicular Technology Conference (VTC)'17*, 2017.
- [28] Y. Yoon, S. Park, and J. Kim, "Empirical Model Including the Statistics of Location Variability for the Over-Rooftop Path in the 32 GHz Band," *IEEE Access*, vol. 8, pp. 77 263–77 271, 2020.
- [29] P. Sharma, T. Atalay, H.-A. Gibbs, D. Stojadinovic, A. Stavrou, and H. Wang, "5G-WAVE: A Core Network Framework with Decentralized Authorization for Network Slices," in *Proc. of IEEE INFOCOM'24*, 2024.
- [30] J. L. G. L. Qingyu Song, Juncheng Wang and H. Xu, "A Learning-Only Method for Multi-Cell Multi-User MIMO Sum Rate Maximization," in *Proc. of IEEE INFOCOM'24*, 2024.
- [31] Z. Z. Y. W. G. C. Jinlong E, Lin He and W. Chen, "AggDeliv: Aggregating Multiple Wireless Links for Efficient Mobile Live Video Delivery," in *Proc. of IEEE INFOCOM'24*, 2024.
- [32] K. Haneda, J. Zhang, L. Tan, G. Liu, Y. Zheng, H. Asplund, J. Li, Y. Wang, D. Steer, C. Li, T. Balercia, S. Lee, Y. Kim, A. Ghosh, T. Thomas, T. Nakamura, Y. Kakishima, T. Imai, H. Papadopoulos, T. S. Rappaport, G. MacCartney, M. Samimi, S. Sun, O. Koymen, S. Hur, J. Park, C. Zhang, E. Mellios, A. Molisch, S. Ghassamzadeh, and A. Ghosh, "5G 3GPP-Like Channel Models for Outdoor Urban Microcellular and Macrocellular Environments," in *Proc. of IEEE Vehicular Technology Conference (VTC)'16*, 2016.
- [33] ETSI, "3GPP TR 38.901 version 14.3.0 Release 14," 2018.
- [34] D. Chizhik, J. Du, and R. A. Valenzuela, "Universal Path Gain Laws for Common Wireless Communication Environments," *IEEE Trans. Antennas Propag.*, vol. 70, no. 4, pp. 2928–2941, 2022.
- [35] M. Ghoshal, I. Khan, Z. J. Kong, P. Dinh, J. Meng, Y. C. Hu, and D. Koutsonikolas, "Performance of Cellular Networks on the Wheels," in *Proc. of ACM IMC'23*, 2023.
- [36] D. Chizhik, J. Du, G. Castro, M. Rodriguez, R. Feick, and R. Valenzuela, "Path Loss Measurements and Models at 28 GHz for 90% Outdoor Suburban Coverage," in *Proc. of IEEE International Symposium on Antennas and Propagation (ISAP)'18*, 2018.
- [37] NYC Parks, "NYC Tree Map," 2023.
- [38] NYC Mayor's Office of the CTO, "The New York City Internet Master Plan," 2020.